Available online at www.eccomasproceedia.org
Eccomas Proceedia COMPDYN (2017) 2431-2448

ECCOMAS
Proceedia

COMPDYN 2017
6th ECCOMAS Thematic Conference on
Computational Methods in Structural Dynamics and Earthquake Engineering
M. Papadrakakis, M. Fragiadakis (eds.)
Rhodes Island, Greece, 15–17 June 2017

TRADITIONAL MASONRY ARCHES AND DOMES WITH FICTILE TUBULES IN MEDITERRANEAN SEISMIC AREAS: ADVANCED NUMERICAL MODELS AND EXPERIMENTATION

S. Tiberti[1], C. Scuro[2], R. Codispoti[2], R.S. Olivito[2], G. Milani[1]

[1] Department of Architecture, Built Environment and Construction Engineering, Politecnico di Milano
Piazza Leonardo Da Vinci 32, 20133 Milan, ITALY
{simone.tiberti,gabriele.milani}@polimi.it

[2] Department of Civil Engineering, University of Calabria
Via Ponte P. Bucci (cubo 39B), 87036 Rende (CS), ITALY
{carmelo.scuro, rosamaria.codispoti, renato.olivito}@unical.it

Keywords: Fictile Tubules, Masonry, Experimental Tests, Homogenization, Nonlinear Static Analyses.

Abstract. *Archaeological discoveries made all over the Mediterranean area – highly prone to earthquakes – have highlighted the use of fictile tubules for the building of walls and domes in thermal baths and masonry kilns since the Roman Empire. Fictile tubules are cylindrical clay bricks with a hollow conformation that ensures lightness and provides thermal insulation for the structural element. This well serves the purposes of thermae and kilns, since heat dispersion affects their functionality. Fictile tubules were usually either embedded in mortar or assembled with a female-male coupling system. This paper investigates the behavior of structural elements employing such technology via experimental tests and numerical analyses. First, tubules and mortar are considered separately. The behavior of each element is investigated by performing compressive and three-point bending tests to define their mechanical properties. These are inserted into existing material models in the 3D FE software Abaqus. They are then calibrated in order to match the experimental tests. Second, the mechanical behavior of an elementary cell composed of tubules embedded in mortar is investigated. Tensile and compressive numerical tests are performed via Abaqus to derive the mechanical behavior of this homogenized material. Finally, linear and nonlinear static analyses are performed on an arch through the exploitation of the new homogenized material.*

Peer-review under responsibility of the organizing committee of COMPDYN 2017.
doi: 10.7712/120117.5579.17425

1 INTRODUCTION

Calabria is a region located in Southern Italy which is often subject to destructive earthquakes, often leading to the loss of human lives. Among the many powerful seismic shocks that have occurred in this region over history, one in particular stands out for its deadliness. On December 28, 1908 the cities of Messina and Reggio Calabria were struck by an earthquake characterized by a moment magnitude of 7.1, with an estimated death toll of 100,000. While most of the buildings were obliterated, a few resisted where hollow clay bricks called "fictile tubules" were used in the construction. Indeed, during the reconstruction of the city in 1909, an engineer by the name Pasquale Frezza proposed the creation of an aseismic house with walls made of such hollow bricks [1].

Fictile tubules are ceramic elements introduced during the Roman Empire in Calabria and neighboring regions, which were part of existing trade routes between Africa and Italy [2]. They have been used since the third century A.D. to build barrel and cross vaults, domes and partition walls. The traditional technique for creating fictile tubules requires that the potter removes impurities and air from the clay – the raw material of which these objects are made. The clay is then put on the potter's wheel and the potter gives shape to the object by applying pressure with moistened hands (Fig. 1a) [2].

Often fictile tubules are characteristic of structures in archaeological sites or buildings protected by superintendence of cultural heritage. Samples from existing sites are few, hence new fictile tubules (NFTs) were created by the ceramic industry (Fig. 1b). NFTs specimens were produced with newer and faster techniques using special machines, thus reducing preparation time, then completed on the potter's wheel.

The shape of NFTs was inspired by common shapes of tubules in Calabria. A thorough investigation on the geological map of clays in the region was conducted in order to find buildings erected with fictile tubules. In the whole area of Calabria this study identified 52 structures built with this technique, which are widespread and not unique examples [3]. The study subdivided the tubules in Calabria into three categories characterized by shape and size. Each type is often similar to tubules found in adjoining Italian regions. Fictile tubules in Northern Calabria display a cylindrical, truncated cone and amphora shapes, with a base to height ratio approximately equal to 1:3 and a height ranging from 15 to 20 cm (Fig. 1c-1). Conversely, tubules in the provinces of Crotone, Vibo Valentia and Catanzaro are shorter than the previous ones, with a base to height ratio equal to 1:2 and a height varying from 12 to 16 cm. These are characterized by a cylindrical and truncated cone shape (Fig. 1c-2) [4]. Moreover, tubules in and around Reggio Calabria (Roccella Jonica, Locri, Gerace, Caulonia, Siderno, Riace) are similar to those found in Sicily. These tubules are low and squat, presenting a cylindrical shape, with a base to height ratio equal to 1:1 and a height between 7 and 10 cm (Fig. 1c-3) [5].

The structures investigated in the aforementioned study were added to a summary abacus, and it must be noted that they were built before 1908. Also, barrel vaults and other structures were placed in areas always struck by powerful earthquakes, albeit the moment magnitude in those areas never reached a value of 7. They usually withstood quakes without showing serious damage, thus highlighting the importance of using this technique in zones with high seismic risk – as did engineer Frezza with his patent in 1909. Fictile tubules allowed the building of vertical structures, vaults and domes characterized by medium-to-high resistance while decreasing the weights and participating mass during the earthquake, in addition to limiting the formation of cracks and the instability of structures.

a) b) c)

Figure 1: a) Preparation of fictile tubules with the traditional technique; b) New fictile tubules made in industry; c) Different types of fictile tubules in Calabria.

2 EXPERIMENTAL PROGRAM

The aim of the experimental program was to independently investigate the mechanical properties of fictile tubules and mortar. All experimental tests were conducted at the Materials and Structures Engineering Laboratory of Civil Department of University of Calabria. The experimental mechanical properties obtained were later used to calibrate the numerical models of the two materials.

2.1 Materials and tests set-up

Uniaxial compression tests were performed on five NFTs (Fig. 2a) replicating the traditional tubules of Northern Calabria. The testing machine used for the tests operated with a displacement control. The position and the lowering of the loading plate was provided at any instant and controlled through displacement sensors connected to the CPU of the test machine control panel. The strain of the specimens was measured via strain gauges. The cylindrical loading plate has a diameter equal to 15 cm and a height equal to 2.5 cm (Fig. 2b). The compressive tests were performed with a crosshead speed equal to 1 mm/min. The geometric properties of the five specimens are listed in Table 1.

Specimen	Weight [kg]	Height [mm]	Diameter [mm]	Resistant area A_{res} [mm^2]
C1	0.253	137	65	584.04
C2	0.255	134	65	584.04
C3	0.248	136	66	588.75
C4	0.262	137	58	435.68
C5	0.267	138	58.5	439.6

Table 1: Characteristics of specimens used

The mortar tested was the M 2.5 labelled as "bastarda" according to Table 11.10.IV of the Italian Building Code [6]. Three-point bending and compressive tests were carried out in accordance with EN 1015/11 [7] on four specimens prepared in the laboratory. First, as recommended by standards, three-point bending tests were performed on prism-shaped specimens with dimensions equal to 160x40x40mm^3 (Fig. 2c), then compressive tests were carried out on the halves originating from the previous tests.

The three-point bending testing machine is composed of three steel rollers: two of them support the specimen and have a mutual distance of about 100 mm, while the third acts on the upper side and is devoted to the application of the load (Fig. 2d). The load was applied at a uniform rate with a speed of 10 N/s.

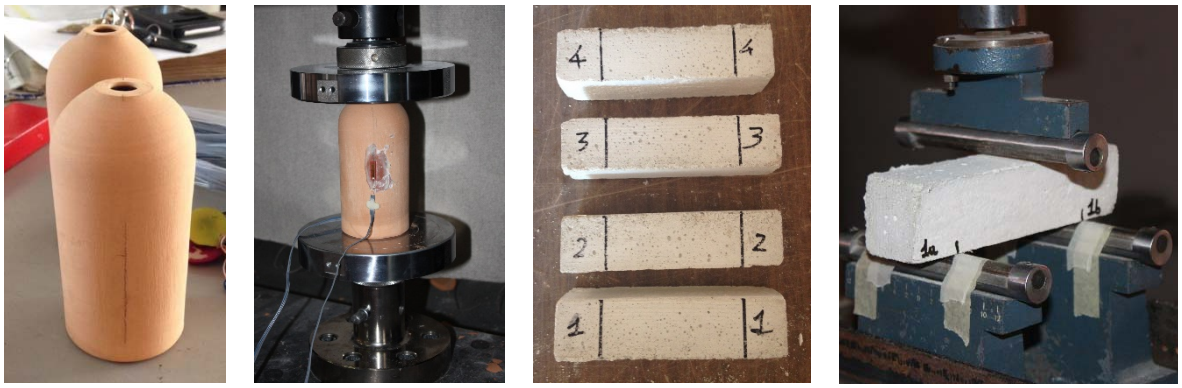

a) b) c) d)

Figure 2: a) Carosello specimens; b) Set-up compression machine; c) Specimens of mortar; d) Set-up three points bending machine

2.2 Experimental results

The mechanical properties obtained from the experimental tests are compressive strength and elastic modulus for fictile tubules and compressive strength and flexural tensile strength (f_{fm}) for mortar. The force-displacement diagrams of compressive tests on fictile tubules are plotted in Fig. 3a. All specimens clearly display a brittle mechanical behavior with a strong linearity prior to failure. Also, the presence of strain gauges allowed the evaluation of a constitutive law for the fictile tubules. Figure 3b shows the compressive stress-strain diagram related to specimen C1.

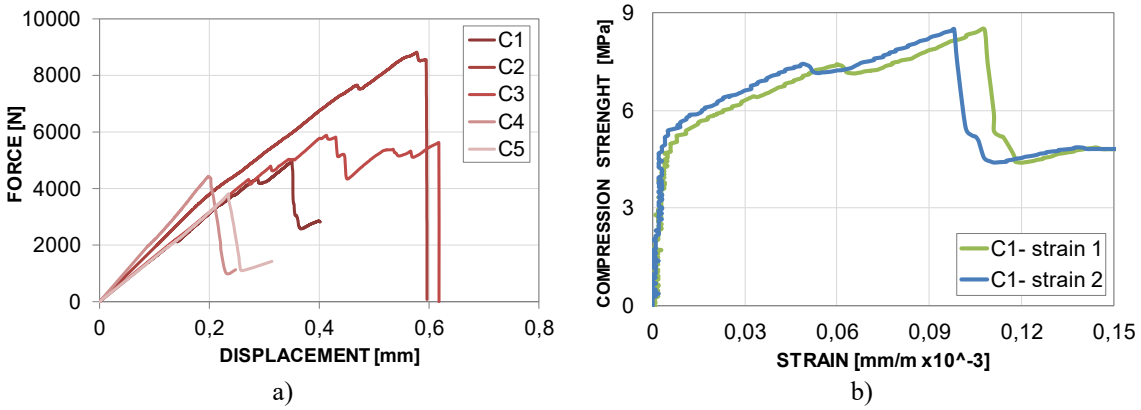

a) b)

Figure 3: Results of compressive tests on fictile tubules: a) Force-displacement diagrams; b) Compressive stress-strain diagram.

For the mortar specimens, force-displacement diagrams for both flexural and compressive tests are plotted in Fig. 4. Each specimen was weighed and measured. The flexural tensile strength was determined according to [7]:

$$f_{fm} = 1.5 \cdot \frac{Fl}{d^3}$$

where F is the maximum force, l is the length between the two supporting rollers equal to 100 mm (Fig. 2d) and d is the transversal dimension of the prism equal to 40 mm. The tensile strength was calculated as 80% of the flexural tensile strength, whereas the compressive strength was evaluated as the ratio between the maximum force and the cross section area perpendicular to the load application.

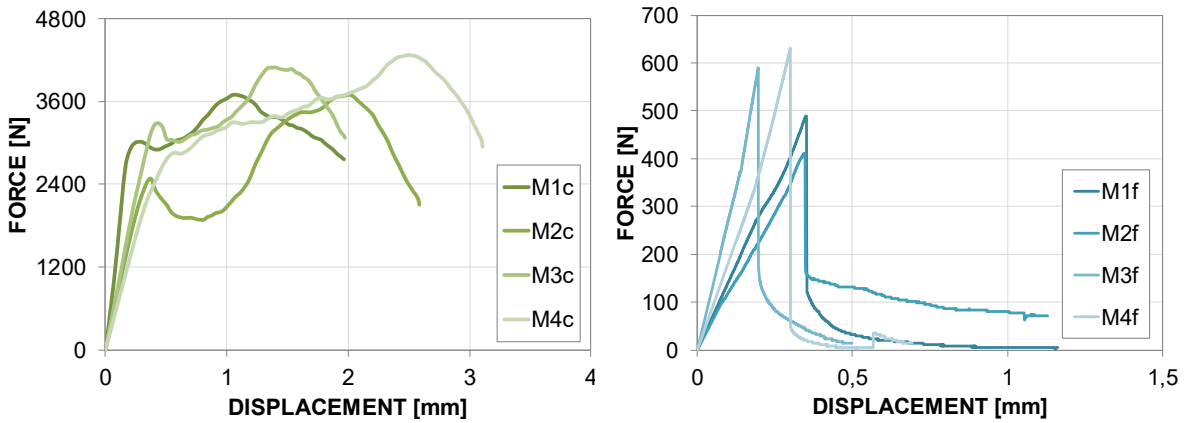

Figure 4: Results of experimental tests on mortar: a) Force-displacement diagrams related to compressive tests; b) Force-displacement diagrams related to three-point bending tests.

The average values of mechanical properties obtained from experimental tests on mortar and fictile tubules are summarized in Table 2.

	Compressive strength [N/mm^2]	f_{fm} [N/mm^2]	f_{tm} [N/mm^2]	Young's modulus [MPa]
Mortar	2.46	1.25	1	300
Fictile tubules	10.5	-	-	4455

Table 2: Mechanical properties obtained from experimental tests

3 NUMERICAL MODELS

The commercial finite element software Abaqus was employed in this paper. Numerical models for fictile tubules and the mortar were independently developed and validated by simulating the experimental tests. Then homogenization was performed on an elementary cell to obtain a single material able to describe the mechanical behavior of a structure consisting of fictile tubules and mortar. Homogenization is a common technique used for the modelling of masonry and masonry-like structures [8].

3.1 Fictile tubules

The dimensions for the numerical model of the fictile tubule are listed in Table 3. A finite element mesh was adopted consisting of 8305 nodes and 5784 elements (5608 bricks C3D8 and 176 wedges C3D6) as shown in Fig. 5a.

Specimen	Height [mm]	Diameter [mm]	Resistant area A_{res} [mm^2]
C1	137	65	584.04
C2	134	65	584.04
C3	136	66	588.75
C4	137	58	435.68
C5	138	58.5	439.6
Numerical model	133.3	62	505.22

Table 3: Characteristics of numerical model compared to specimens

The brittle cracking model provided by Abaqus [9] was employed to simulate the mechanical response of the tubules. Although it was conceived to describe the brittle behavior of concrete, this model is suitable to describe all materials displaying brittle cracking in tension. Conversely, linear elasticity is assumed in compression. A cracking behavior based on Mode I fracture energy was used for the tubule. Also, a brittle failure criterion is included in the model, thus allowing removal of elements from the mesh and a direct observation of crack initiation and formation in the model. Furthermore, taking into account the fact that postcracked behavior includes Mode II as well as Mode I, a shear retention model in which the postcracked shear stiffness is defined in power law form as a function of the opening strain across the crack.

The elastic properties and the main parameters of the brittle cracking model are shown in Table 4.

Young's modulus [MPa]	Poisson's ratio [-]	Tensile failure stress [MPa]	Mode I fracture energy [N/mm]	e	p	Direct cracking failure displacement [mm]
4200	0.15	3	0.1	0.05	1	0.01

Table 4: Main properties for the fictile tubule.

The experimental compressive test was replicated via a quasi-static analysis. As in the physical test, a speed of 1 mm/min was applied to the loading plate, which was modelled as a discrete rigid element. The interaction between the tubule and the loading plate was modelled with the general contact algorithm available in Abaqus, setting a tangential friction coefficient equal to 0.4 and a normal behavior based on the "hard contact" feature.

The force-displacement diagram for the numerical model is plotted against the area of the experimental ones in Fig. 5b, and in Fig. 5c-5d the failure mechanism developed by the tubule is shown.

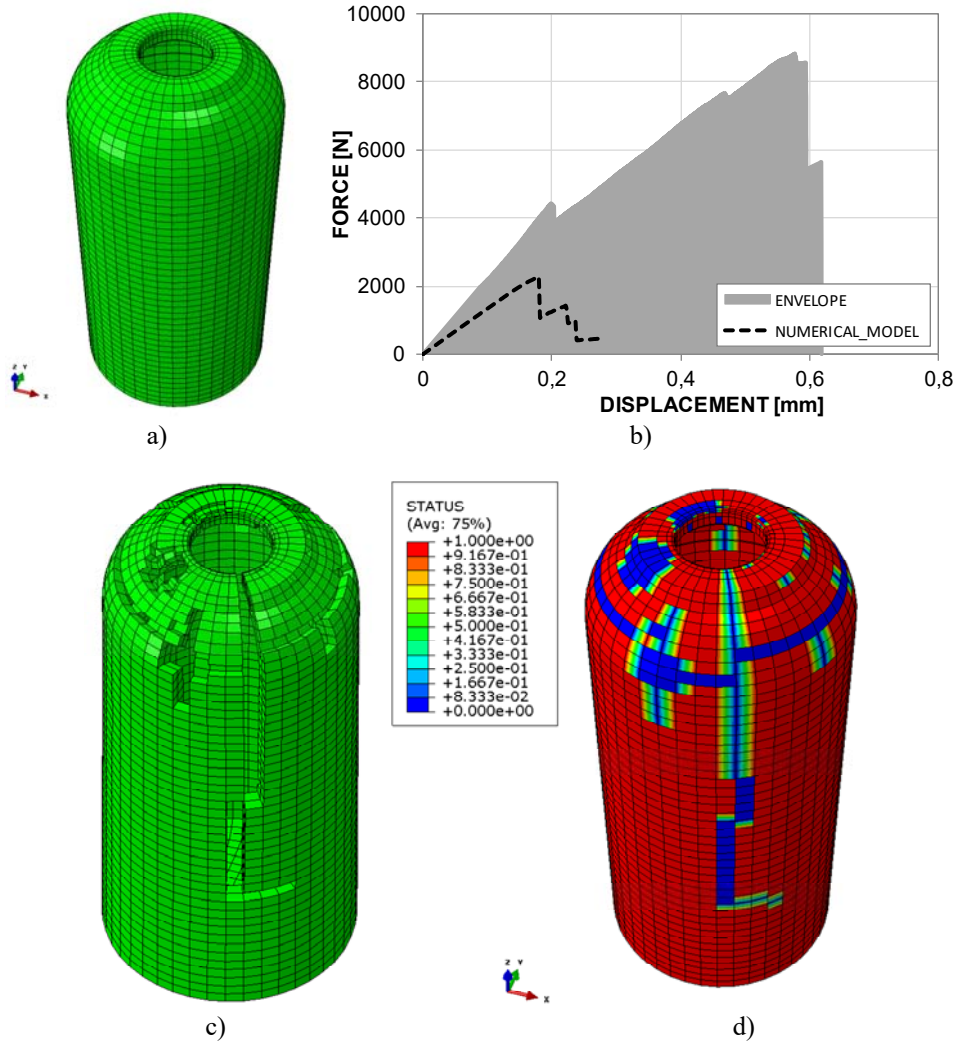

Figure 5: a) Fictile tubule; b) Force-displacement diagrams; c); Failure mode; d) Crack formation (in blue).

3.2 Mortar

A computational model for the mortar was created aiming at the simulation of the three-point bending tests, presenting the same dimensions of the specimens used in the tests (160x40x40 mm^3). A finite element mesh consisting of 1701 nodes and 7737 tetrahedron C3D4 elements was adopted, as shown in Fig. 6a.

The concrete damaged plasticity model (CDP) available in Abaqus [9] was used for replicating the behavior of mortar. Due to its versatility, it befits the characterization of quasi-brittle materials exhibiting damage, such as mortar. Different inelastic behavior for tension and compression can be assumed, and two distinct scalar parameters can be introduced to define damage in tension and compression.

This model also requires the definition of few other parameters for a full description of the material, and they are listed in Table 5.

Symbol	Name	Description	Default value
ϵ	Eccentricity	Distance between the points of intersection with the *p*-axis of the cone and the hyperbola (in the *p*-*q* plane)	0.1
f_{b0}/f_{c0}	Strength ratio	Ratio between the biaxial and uniaxial compression strength	1.16
ψ	Dilation angle	Angle due to a variation in volume of the material following the application of a shear force	7°
K_c	-	Ratio between distance from the hydrostatic axis of the maximum compression and traction respectively	0.666

Table 5: Concrete damaged plasticity parameters.

A further quantity, called "viscosity parameter", was required. It is related to the use of a viscoplastic regularization of the constitutive equation, aimed at overcoming possible severe convergence difficulties due to the softening behavior and stiffness degradation of the material. However, since the numerical analysis is run under Abaqus/Explicit, the parameter was ignored by the software.

The tensile behavior was expressed in terms of tensile strength and Mode I fracture energy, whose values are presented in Table 6 along with the Young's modulus and Poisson's ratio. The damage parameter in tension was expressed as a function of displacement and its evolution is also displayed in Table 6.

Young's modulus [MPa]	Poisson's ratio [-]	Tensile strength [MPa]	Mode I fracture energy [N/mm]	Displacement [mm]	Damage parameter [-]
300	0.2	0.4	0.02	0 0.2	0 0.99

Table 6: Tensile behavior parameters.

The compressive constitutive law was derived from the force-displacement diagrams resulting from the compressive tests, with a peak value of 2.46 MPa (Fig. 6b).

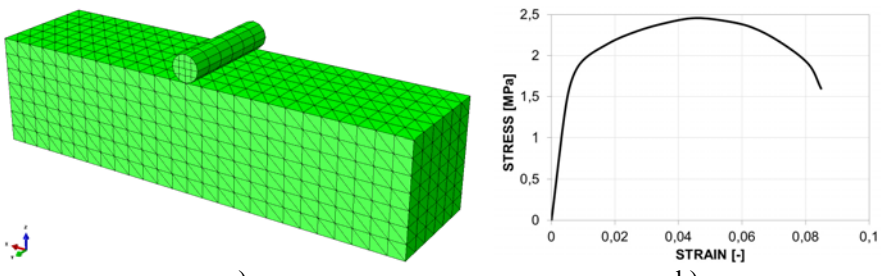

a) b)

Figure 6: a) Mortar specimen; b) Constitutive law in compression.

A quasi-static analysis was run to replicate the three-point bending test. Mirroring the experimental condition, a vertical load was applied at a speed of 10 N/s, as requested by [7]. Only the loading roller was modelled as a discrete rigid element, while the two supporting roller

were substituted by a simple support constraint. The interaction between the loading roller and the mortar specimen was modelled again with a general contact algorithm, imposing a tangential friction coefficient of 0.6 and again making use of the "hard contact" for the normal behavior. The distortion control algorithm available in Abaqus was exploited in order to help the analysis reach convergence, with the distortion control length assumed as 0.01.

The force-displacement diagram for the numerical model is plotted against the envelope of the experimental ones in Fig. 7a, and the output at failure is displayed in Fig. 7b.

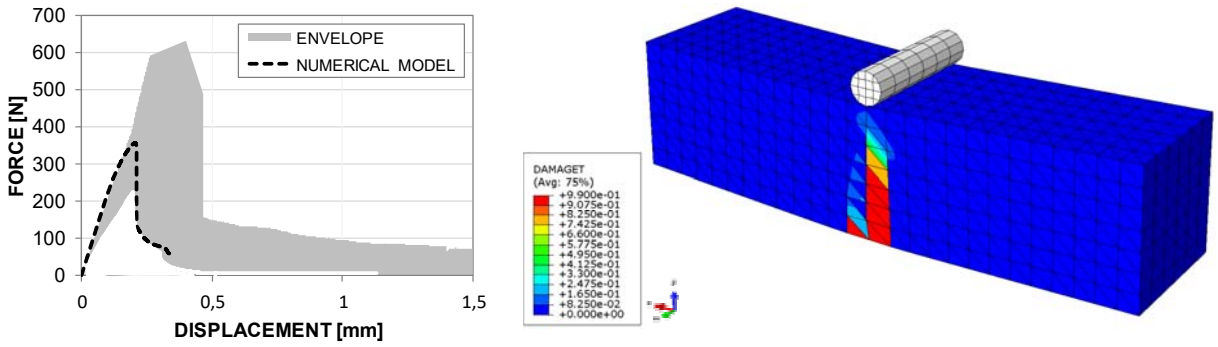

a) b)

Figure 7: a) Force-displacement diagrams; b) Failure mode.

3.3 Elementary cell

In order to derive homogenized properties for the two materials, a numerical model of an elementary cell was created. This cell consisted of one tubule embedded in mortar and surrounded by four quarters of tubules. The finite element mesh presented 27920 nodes and 60599 elements (49118 tetrahedron C3D4 for the mortar, and 11014 bricks C3D8 and 467 wedges C3D6 for the tubules) as shown in Fig. 8a. Perfect adherence between tubules and mortar was considered; therefore tie constraints were set between mortar and each element. Uniaxial compressive and tensile tests were performed on the elementary cell, by applying different displacements along the X axis in tension and compression using a numerical loading plate, modelled as a discrete rigid element. The interaction between the cell and the plate was modelled with a general contact algorithm, imposing a tangential friction coefficient of 0.4 and making use of the "hard contact" for the normal behavior. The force-displacement diagrams of the two uniaxial tests are shown in Fig. 8b and 8c, and the failure modes in compression and tension are shown in Fig. 8d and 8e respectively.

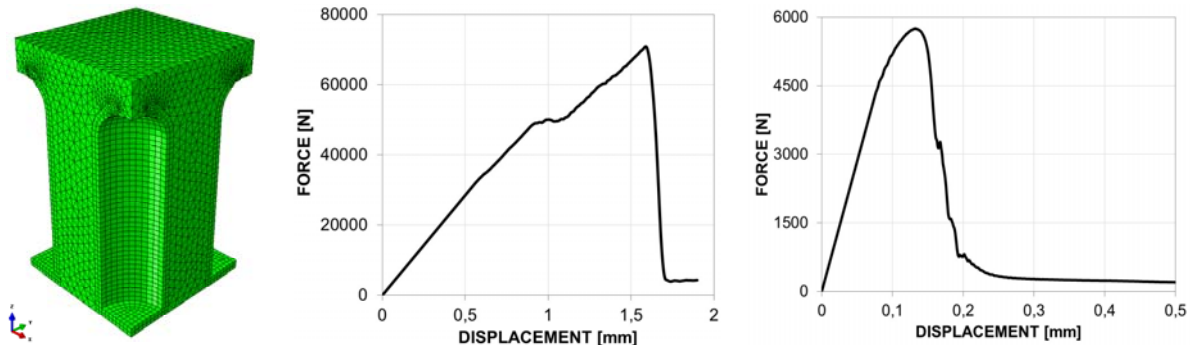

a) b) c)

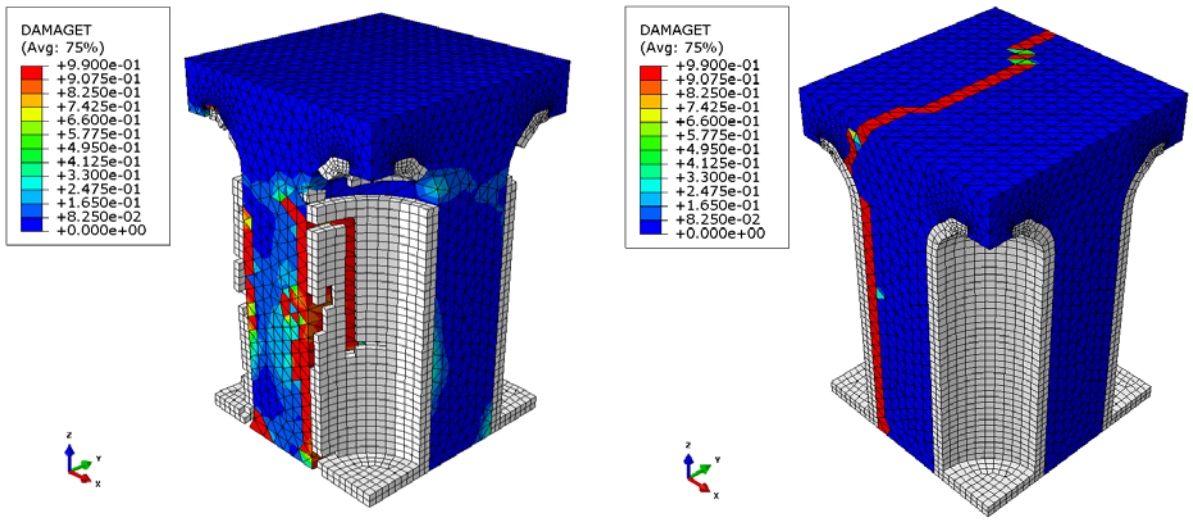

d) e)

Figure 8: a) Finite element mesh for the heterogeneous elementary cell; b) Force-displacement diagram in compression; c) Force-displacement diagram in tension; d) Failure output in compression; e) Failure output in tension.

The failure mode in compression involved damage in mortar and crushing of the tubules, while the failure mode in tension showed the full development of a crack only in the mortar, with the tubules left intact. Moreover, both diagrams displayed a clear brittle mechanical behavior for the cell. Due to this fact, the homogenized material was conceived using the brittle cracking model previously described. The chosen main parameters for the model are listed in Table 7.

Young's modulus [MPa]	Poisson's ratio [-]	Tensile failure stress [MPa]	Mode I fracture energy [N/mm]	e	p	Direct cracking failure displacement [mm]
690	0.15	0.62	0.05	0.05	3	0.03

Table 7: Main properties for the homogenized material.

The numerical model for the homogenized numerical cell used a different mesh with respect to the previous case, consisting of 18642 nodes and 15721 elements (15114 bricks C3D8 and 607 wedges C3D6), as shown in Fig. 9a. The comparison between the heterogeneous and the homogenized materials in terms of force-displacement diagrams is shown in Fig. 9b and 9c, and the outputs at failure for the homogenized case are shown in Fig. 9d and 9e.

The diagrams in compression followed the same initial elastic branch in both cases. While the homogeneous diagram evolved along that branch until sudden failure occurred, the heterogeneous one started deviating when a certain value of displacement was attained due to the damage in the mortar. After a small plateau, the diagram again evolved along a line with the same slope of the elastic branch, and then sudden failure occurred. It must be noted that failure in both cases occurred with the same trend. While there was only a fair correspondence between the two cases, the homogenized model correctly grasped the overall mechanical behavior in compression.

The diagrams in tension followed again the same initial elastic branch in both cases. The heterogeneous diagram had a more regular evolution, after which sudden failure occurred, whereas the homogeneous one showed a clearer brittle behavior. This was certainly due to the fact that in the heterogeneous case the mortar employed a plastic model, hence the regular

evolution of the diagram, while the homogenized material was purely brittle thus leading to a true brittle failure in the model. In both cases a small knee appeared during the sudden decrease in the diagram. Again, despite only a fair correspondence of the two diagrams, the homogenized material was able to describe the overall behavior in tension.

The failure mode in compression showed the crushing of the homogenized material in correspondence of the loading plate (right face in Fig. 9d), in a fashion similar to the one for the heterogeneous case. The failure mode in tension displayed the formation of a full crack at the midsection of the homogenized cell, as it had to be expected since there was no more distinction between mortar and tubules.

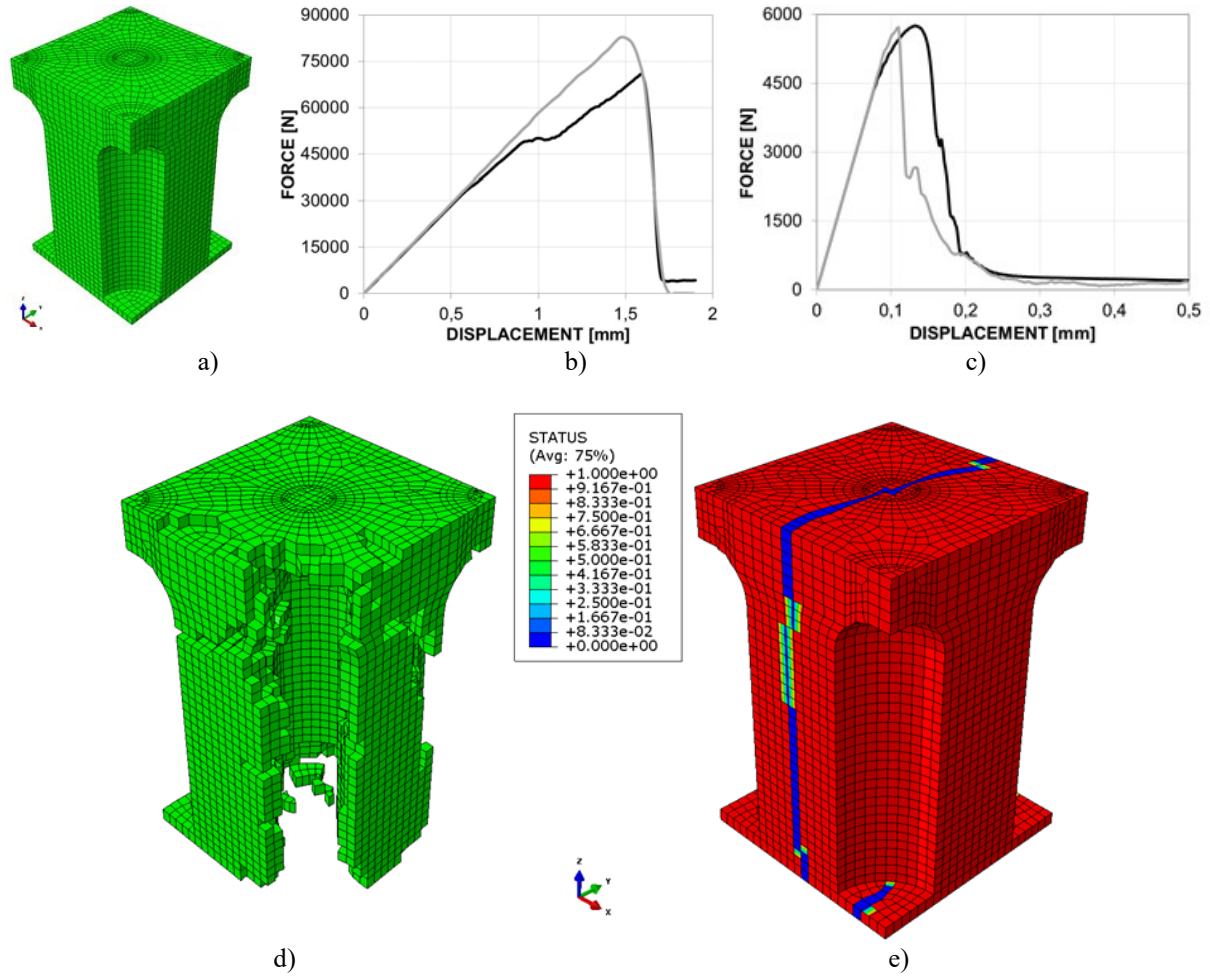

Figure 9: a) Finite element mesh for the homogeneous elementary cell; b) Force-displacement comparison in compression (homogeneous in grey); c) Force-displacement comparison in tension (homogeneous in grey); d) Failure output in compression; e) Failure output in tension.

4 NUMERICAL INVESTIGATIONS OF AN ARCH

A numerical model of an arch made of mortar and fictile tubules was created to further observe the response of the homogenized material, and to investigate the behavior of an actual structure displaying this building technique.

The arch presented 32 rows of tubules, placed in a staggered way (each row consisted either of 6 or 7 elements). The finite element mesh consisted of 75266 nodes and 88958 elements (60046 tetrahedron C3D4 for the mortar, and 28496 bricks C3D8 and 416 C3D6 for the tubules), as shown in Fig. 10. The arch was considered simply supported to the ground.

Linear and nonlinear static analyses were performed on the arch, both employing the homogenized material model and considering the two materials with their own properties. Nonlinear static analyses are also known as "pushover analyses" and have been largely employed to investigate the behavior of masonry structures under horizontal actions in a rather simple way [10] [11].

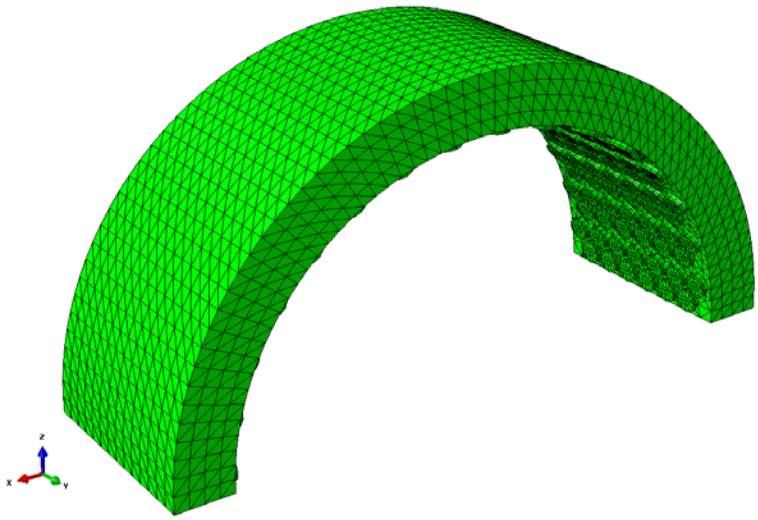

Figure 10: Finite element model for the arch.

4.1 Linear static analyses

A vertical displacement of 5 mm was applied at the keystone extrados section. Fig. 11 shown the stress map of the two cases when the materials were considered linear elastic (which means removing brittle cracking and CDP in both cases). A comparison in terms of damage maps is shown in Fig. 12 for increasing values of vertical displacement at the keystone.

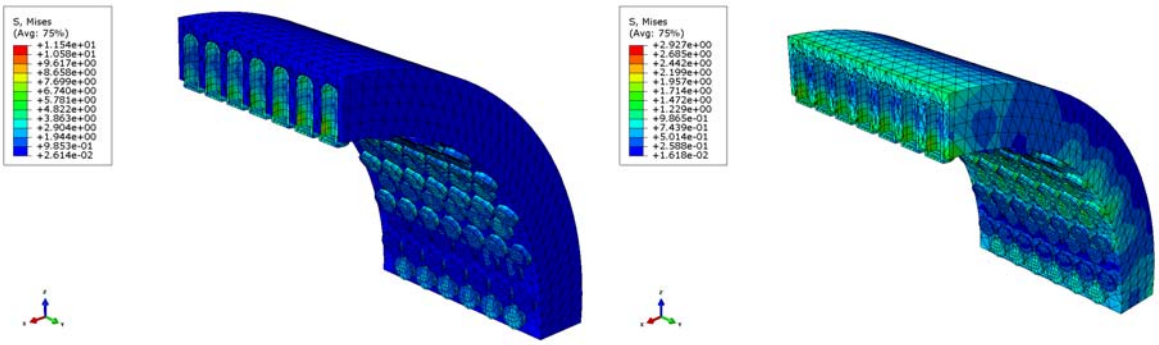

a) b)

Figure 11: Stress maps for the linear static analyses with elastic materials: a) heterogeneous case; b) homogeneous case.

Except for edge effects in the mortar, the stress state in the fictile tubules was similar for the two cases, again demonstrating the overall correctness of the homogeneous model with respect to the heterogeneous one.

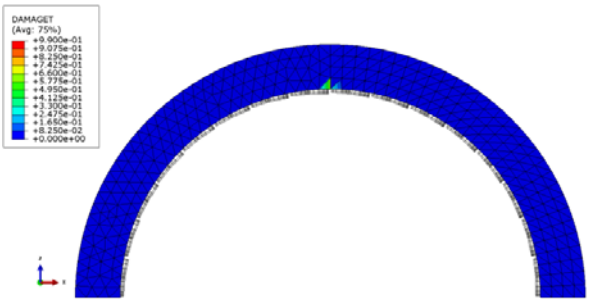

d = 1.25 mm: crack formation at the keystone.

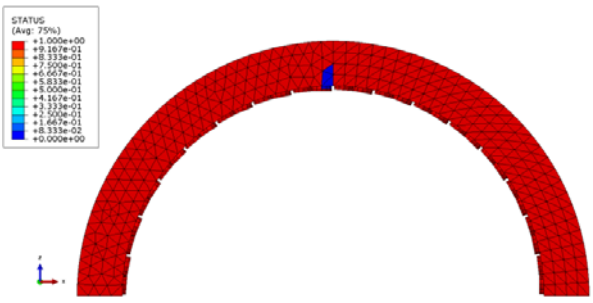

d = 1.25 mm: crack formation at the keystone.

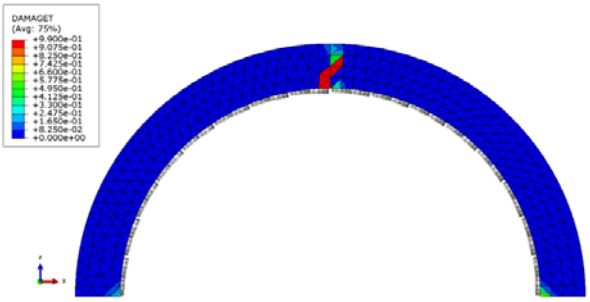

d = 2.125 mm: crack formation at the bases.

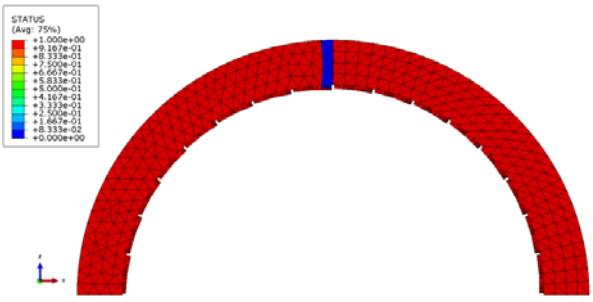

d = 1.875 mm: full development of hinge at the keystone.

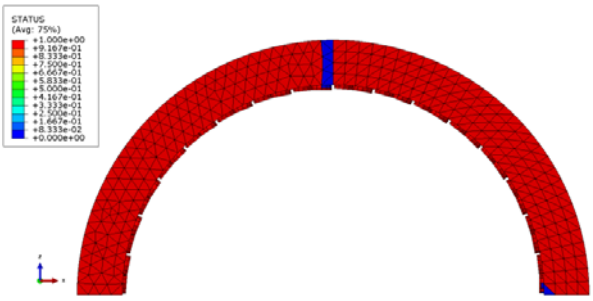

d = 2 mm: crack formation at the base on the right.

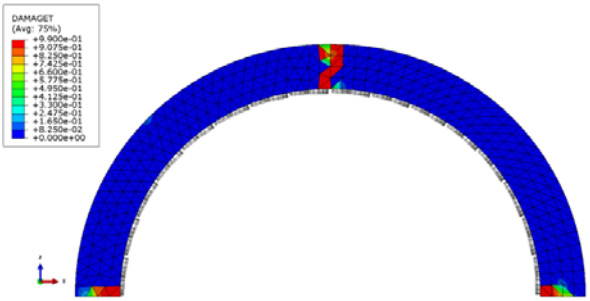

d = 4.375 mm: full development of hinges at the keystone and at the bases.

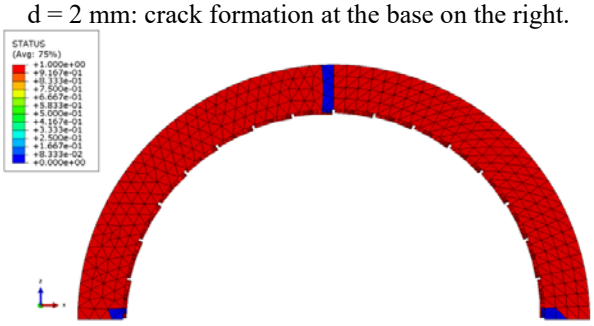

d = 2.125 mm: crack formation at the base on the left.

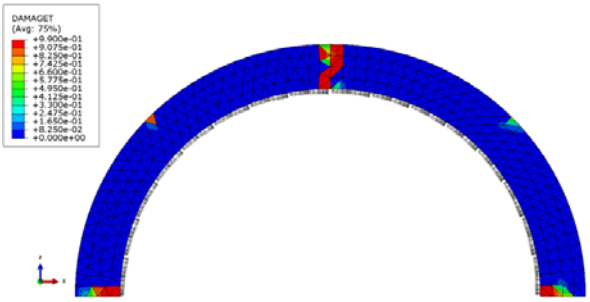

d = 4.5 mm: crack formation at 45° on the left and on the right.

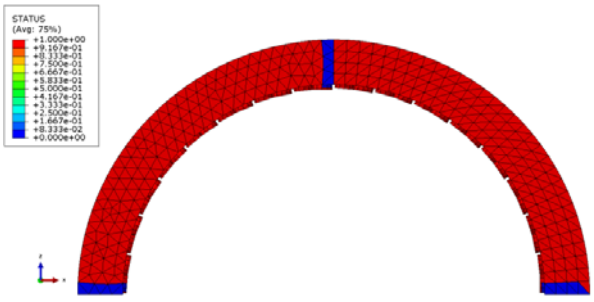

d = 4.5 mm: full development of hinges at the bases.

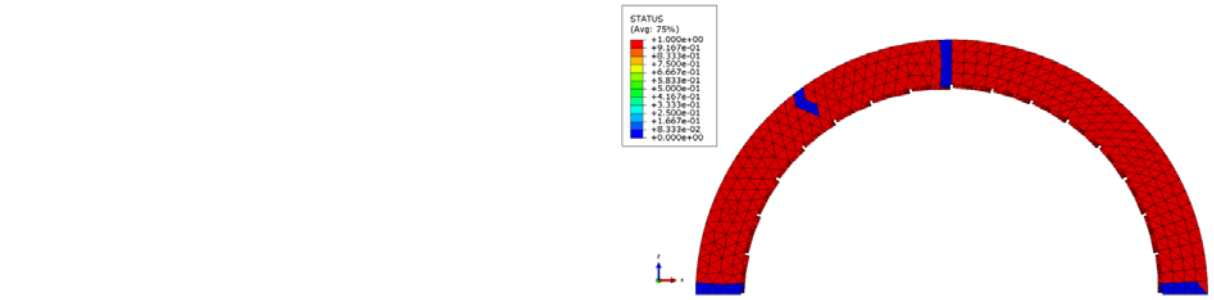

d = 4.625 mm: crack formation at 50° on the left.

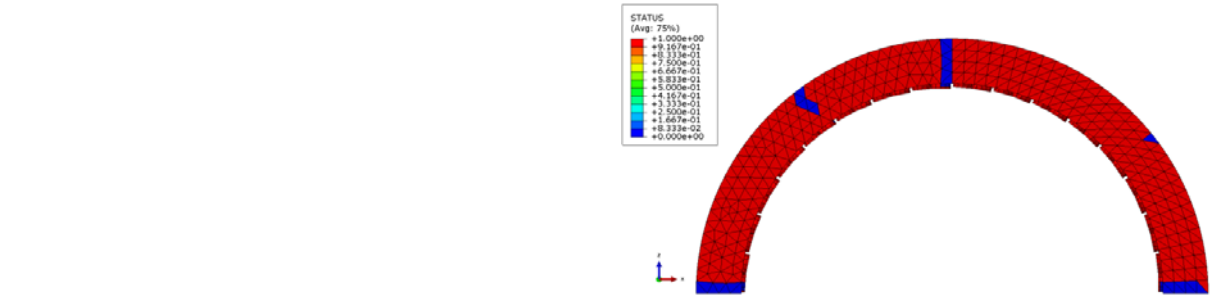

d = 4.75 mm: crack formation at 40° on the right.

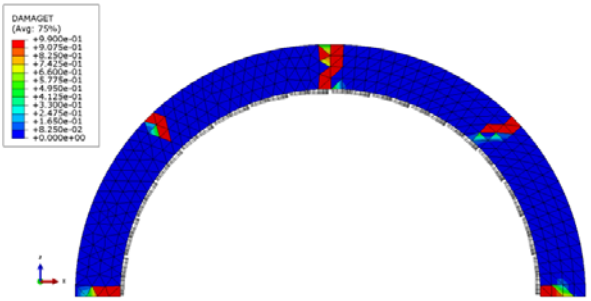

d = 5 mm: final output.

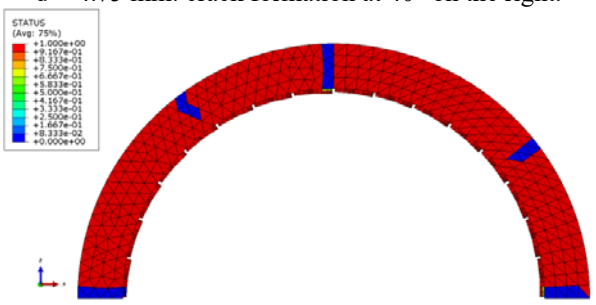

d = 5 mm: final output.

Figure 12: Damage map evolution for the heterogeneous case (left) and damage map evolution for the homogeneous case (right) for the linear static analyses.

With respect to the evolution of the damage maps, the two cases showed a few key differences. At a certain stage, the heterogeneous case displayed the simultaneous development of cracks at the bases and at the keystone, whereas the homogeneous one displayed a clear sequence (keystone first, bases next). Moreover, in the heterogeneous case two more cracks appeared simultaneously at 45°, instead in the homogeneous one they formed one after another and with slight differences in the location. One possible reason for these different outputs could be the asymmetry of the mesh with respect to the vertical axis Z.

4.2 Pushover analyses

The pushover analyses were carried out by applying a load along the positive direction of the X axis. The load distribution varied linearly with the height, and it was increased monotonically until failure occurred. The control point considered for the evaluation of displacements was located at the very center of the keystone extrados section. The comparison between the two cases in terms of force-displacement diagram is plotted in Fig. 13, and a comparison in terms of deformed shapes and damage maps is shown in Fig. 14.

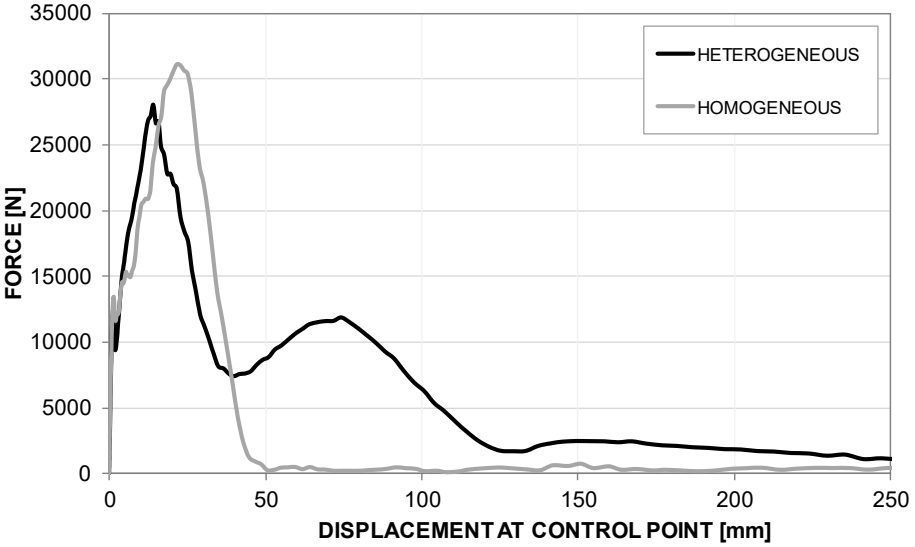

Figure 13: Force-displacement at control point comparison for the nonlinear static analyses.

The heterogeneous diagram evolved in a complex way. After a first relative maximum, it displayed a slight, sudden decrease, followed by a reprisal of increase. Once it attained the maximum force at the bases, another sudden decrease occurred which was followed by a clear stiffness recovery. After reaching a second relative maximum, the diagram decreased once again in a more regular fashion down to low values of the reaction force at the bases, suggesting that a complete mechanism had formed in the arch.

The homogeneous diagram reached a relative maximum and again displayed a slight decrease, albeit smaller than in the previous case. The reprisal of increase occurred once more, but in this case the maximum force attained is higher than the one of the heterogeneous case (31133 N v. 28009 N). Then the diagram displayed a relevant, sudden decrease down to very low values of the reaction force at the bases, suggesting again the formation of a complete mechanism in the arch.

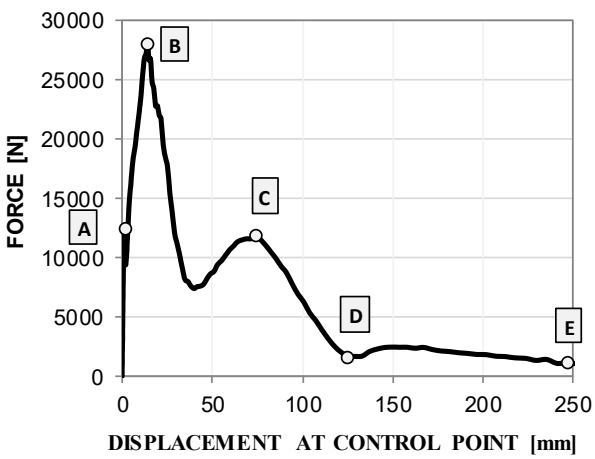

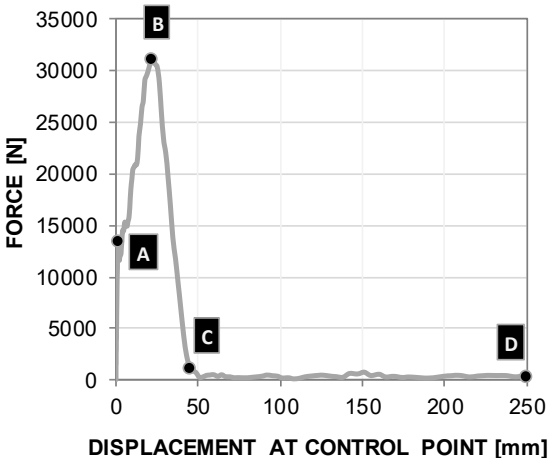

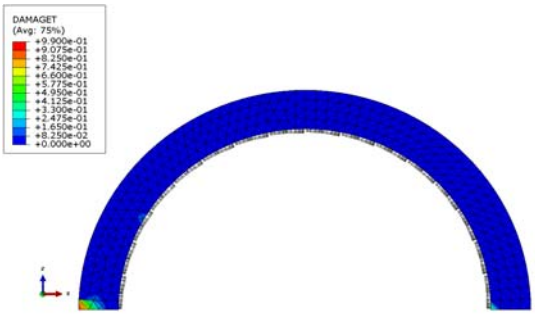

A – First relative maximum: crack formation at the bases.

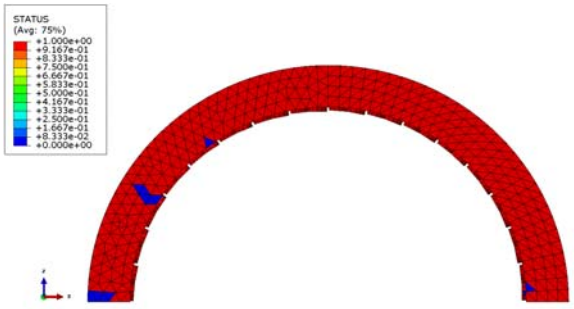

A – First relative maximum: crack formation at the bases and at 30° and 60° on the left.

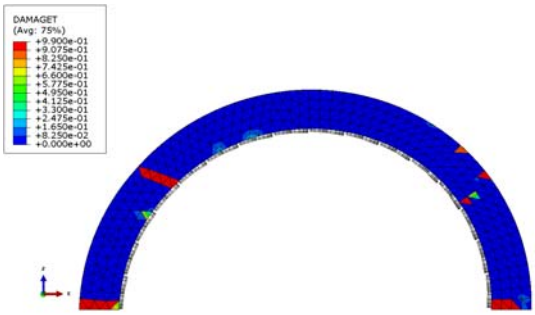

B – Absolute maximum: full development of hinges at the bases and at 35° on the left, crack formation on the right.

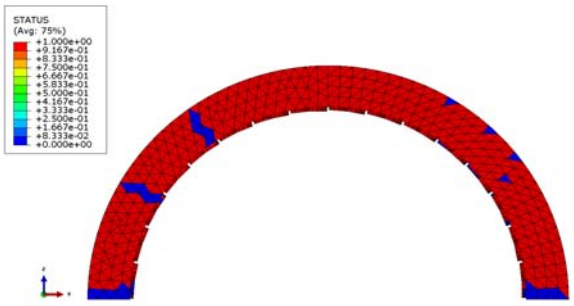

B – Absolute maximum: full development of hinges at the bases and at 30° and 60° on the left, crack formation on the right → MECHANISM.

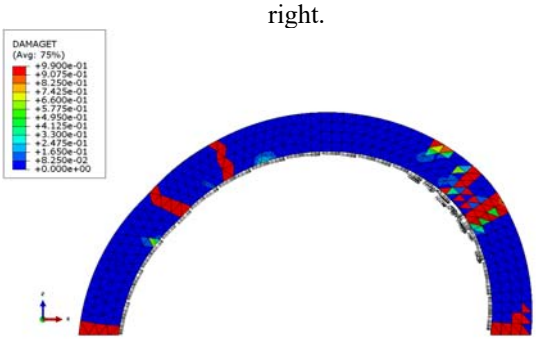

C – Second relative maximum: full development of hinges at 50° on the left and at 40°-45° on the right → MECHANISM.

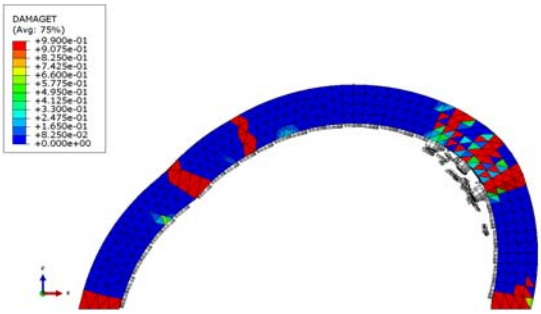

D – Low resistance: further cracks on the right, detachment of tubules.

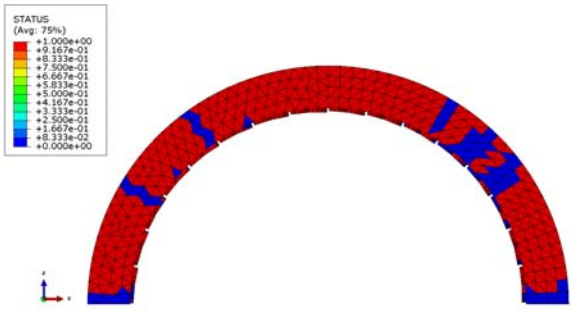

C – Low resistance: full development of hinges at 30°-60° on the right.

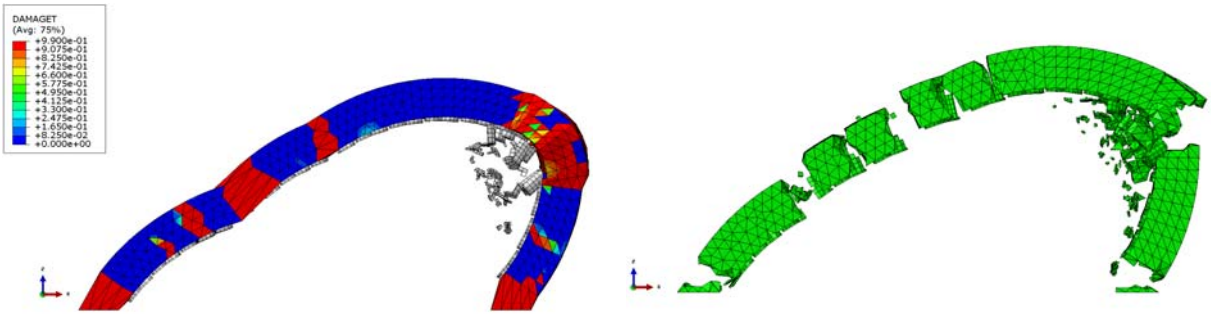

E – Ultimate state: collapse of the arch. D – Ultimate state: collapse of the arch.

Figure 14: Damage map and deformed shape evolution for the heterogeneous case (left) and damage map evolution and final deformed shape for the homogeneous case (right) for the nonlinear static analyses.

Although the evolution of the force-displacement diagrams was different, the damage maps were sufficiently similar in the two cases. The main discrepancy consisted of the stiffness recovery displayed by the heterogeneous diagram, which delayed the formation of the full mechanism, but otherwise a fair correspondence could be noticed between the two cases in general and also in the ultimate state.

5 CONCLUSIONS

Fictile tubules were a common construction technique in Southern Italy. They helped the buildings resisting disastrous earthquakes typical of that region. Different areas presented different shapes of tubules. Fictile tubules and mortar were each experimentally tested to characterize the two materials. Experimental tests were simulated via numerical analyses in Abaqus to obtain mechanical properties with material models available in the software. A numerical model of an elementary cell was created for homogenization purposes. The homogenized material was able to correctly mirror the overall behavior of the two materials placed in full interaction.

Linear static analyses performed on an arch consisting of tubules and mortar showed sufficient accuracy of the homogenized material, albeit displaying a few key differences in terms of damage evolution that could be explained by an asymmetric mesh. Moreover, nonlinear static analyses on the same arch led to slightly different force-displacement diagrams, whilst displaying a similar evolution in damage maps.

Linear and nonlinear static analyses could be repeated using a more regular mesh to check if the discrepancies disappear. As a further development, nonlinear dynamic analyses could be performed using the accelerogram of an earthquake occurred in the region to check the behavior of the arch under seismic actions.

REFERENCES

[1] Central State Archive, Rome, Ministry of Agriculture, Industry and Commerce, the Central Patent Office, patent number 103254 Pasquale Frezza, Laureana di Borrello, Reggio Calabria.

[2] R.S. Olivito, C. Scuro, R. Codispoti, Experimental analysis of typical hollow clay fictile tubules of cultural heritage of Mediterranean area, *Structural Analysis of Historical Constructions: Anamnesis, diagnosis, therapy, controls*, Leuven, Belgium, September 13-15, 2016.

[3] R.S. Olivito, C. Gattuso, C. Scuro, R. Codispoti, Static analysis of barrel vaults built with hollow clay fictile tubules with different geometry, *Proceedings of 6th AIES National Conference*, Naples, Italy, December 10-11, 2015.

[4] C. Gattuso, R.S. Olivito, R. Codispoti, Mechanical characterization of fictile elements typical of Mediterranean architecture, *Proceedings of 4th AIES National Conference*, Naples, Italy, December 12-13, 2013.

[5] R.S. Olivito, C. Gattuso, R. Codispoti, C. Scuro, Analysis of a constructive system using hollow clay elements (Caruselli) in Calabria, *Proceedings of 5th AIES National Conference*, Naples, Italy, December 11-12, 2014.

[6] NTC2008, Norme tecniche per le costruzioni, 2008.

[7] EN 1015/11, Methods of test for mortar for masonry – Part 11: Determination of flexural and compressive strength of hardened mortar.

[8] M. Acito, G. Milani, Homogenization Approach for the Evaluation of Crack Patterns Induced by Foundation Settlement on an Old Masonry Building, *The Open Civil Engineering Journal*, **6 (Suppl. 1-M9)**, 215-230, 2012.

[9] ABAQUS®, Theory manual, version 6.13-2, 2013.

[10] S. Tiberti, M. Acito, G. Milani, Comprehensive FE numerical insight into Finale Emilia Castle behavior under 2012 Emilia Romagna seismic sequence: Damage causes and seismic vulnerability mitigation hypothesis, *Engineering Structures*, **117**, 397-421, 2016.

[11] G. Milani, M. Valente, Comparative pushover and limit analyses on seven masonry churches damaged by the 2012 Emilia-Romagna (Italy) seismic events: Possibilities of non-linear finite elements compared with pre-assigned failure mechanisms, *Engineering Failure Analysis*, **47 (Part A)**, 129-161, 2015.